

Analytical Shaping Method for Low-Thrust Rendezvous Trajectory Using Cubic Spline Functions

Di Wu, Tongxin Zhang, Yuan Zhong, Fanghua Jiang*, Junfeng Li

School of Aerospace Engineering, Tsinghua University, 100084 Beijing, People's Republic of China

Abstract

Preliminary mission design requires an efficient and accurate approximation to the low-thrust rendezvous trajectories, which might be generally three-dimensional and involve multiple revolutions. In this paper, a new shaping method using cubic spline functions is developed for the analytical approximation, which shows advantages in the optimality and computational efficiency. The rendezvous constraints on the boundary states and transfer time are all satisfied analytically, under the assumption that the boundary conditions and segment numbers of cubic spline functions are designated in advance. Two specific shapes are then formulated according to whether they have free optimization parameters. The shape without free parameters provides an efficient and robust estimation, while the other one allows a subsequent optimization for the satisfaction of additional constraints such as the constraint on the thrust magnitude. Applications of the proposed method in combination with the particle swarm optimization algorithm are discussed through two typical interplanetary rendezvous missions, that is, an inclined multi-revolution trajectory from the Earth to asteroid Dionysus and a multi-rendezvous trajectory of sample return. Simulation examples show that the proposed method is superior to existing methods in terms of providing good estimation for the global search and generating suitable initial guess for the subsequent trajectory optimization.

Key words: Trajectory approximation, Analytical shaping method, Cubic spline functions, 3-D multi-revolution rendezvous

Nomenclature

\mathbf{a}	= acceleration vector, [m/s ²]
$\mathbf{a}_i, \mathbf{b}_i, \mathbf{c}_i, \mathbf{d}_i$	= shaping polynomial coefficients of i -th segment
a_t, b_t, c_t	= polynomial coefficients for transfer time constraint, [s]
\mathbf{A}, \mathbf{B}	= matrices in motion equations
c	= number of discrete constrained points
C^2	= set of second-order continuous functions
g_0	= standard acceleration of gravity, [m/s ²]
I_{sp}	= specific impulse, [s]
J	= performance index
m	= spacecraft mass, [kg]
n	= number of finite segments
\mathbf{r}, \mathbf{v}	= spacecraft position and velocity, [m and m/s]
\mathbb{R}	= set of all real numbers
s	= normalized independent variable
S	= domain of independent variable
t	= coordinate time, [s]
T_{max}	= maximum thrust magnitude, [N]
\mathbf{u}	= control vector, [m/s ²]
\mathbf{x}	= state vector
\mathbf{z}	= undetermined parameters

* Corresponding author.

Email addresses: wud17@mails.tsinghua.edu.cn (Di Wu), ztx18@mails.tsinghua.edu.cn (Tongxin Zhang), y-zhong17@mails.tsinghua.edu.cn (Yuan Zhong), jiangfh@tsinghua.edu.cn (Fanghua Jiang), lijunf@tsinghua.edu.cn (Junfeng Li).

Δ_t	=	discriminant for the transfer time constraint
Δ_p	=	discriminant for the semi-latus rectum constraint
ϕ	=	boundary state cost function
φ	=	running cost function
μ	=	gravitational parameter, [m ³ /s ²]
ρ	=	penalty function
ξ	=	shape function
\hbar	=	magnitude of angular momentum
$\boldsymbol{\alpha} = [p, f, g, h, k, L]^T$	=	modified equinoctial orbital elements

Subscripts

f	=	final
\max	=	maximum
\min	=	minimum
opt	=	optimal
r, θ, h	=	components in the radial, in-track, and cross-track directions
0	=	initial

Superscripts

$^{-1}$	=	inverse
$^{(1)}, ^{(2)}$	=	the first and second solution
T	=	transpose
\cdot	=	time derivative
$'$	=	derivative to shaping independent variable

1 Introduction

In the past few decades, the low-thrust propulsion has gained great interest for its specific impulse higher than that of traditional chemical propulsion [1,2] and almost no fuel consumption when using the innovative solar balloons [3] and the electric solar sails [4]. The applications have been sufficiently validated in some practical missions, such as the Hayabusa 2 [5] and BepiColombo [6]. Numerous methods have been proposed for the global search and local optimization of the continuous low-thrust trajectory [7,8,9]. The global search (or preliminary design) usually find the parameters that are critical to the overall performance over a broad search space, for example the rendezvous or gravity-assist sequences and epochs in the deep-space mission scenarios [10,11]. By comparison, the local optimization solves the optimal control problem based on the results of the global search [11], generating the solution that satisfies the first-order necessary conditions (i.e., the Karush-Kuhn-Tucker condition [12] for the direct method). Obviously, accurate evaluation of the local solution can help the global search to find the global optimal solution, which require the local optimal solution algorithm to be extremely fast.

For the general case of low-thrust trajectory in a central gravitational field, the motion equations are not analytically integrable [13,14] and the optimal control problem should be numerically solved by the direct or indirect methods, which are admittedly time-consuming to conduct [7,15]. So far, much effort has been devoted to the approximate or exact analytical solutions for some specific thrust profiles (e.g., the constant tangential thrust [16,17] and radial thrust [18,19]) and for the particular transfers between near-circular orbits [20,21]. These solutions show the effectiveness in fast estimation, but may be far away from the optimal trajectory because their assumptions are only reasonable for limited cases. To approximate the solution with large eccentricity or inclination, some shape-based methods are proposed, such as the exponential sinusoid and logarithmic spiral shapes for the low-thrust interception

[11,19], the inverse polynomial and finite Fourier series shapes for the near-coplanar transfer and rendezvous [22,23], and the pseudo-equinoctial elements (not including the true longitude) and spherical shapes for the three-dimensional (3-D) problems [24]. These methods are used extensively for the mission design in combination with some global search algorithms [25]. However, there are still some common problems to be studied further. One is the shaping optimality for the 3-D multi-revolution rendezvous [26], which has been discussed in [27] and evaluated by solving an equivalent optimal control problem. Moreover, the optimality can be assessed through taking the shape solutions as the initial guesses of the direct and indirect methods [13,27]. Compared with the coplanar case, it is more challenging to design the near-optimal solutions of the 3-D trajectories because of their complexity. Moreover, the satisfaction of the rendezvous time constraint may lead to a nonlinear equation that can be solved by the Newton's method. Since the Newton's method may fail to converge when used to solve the nonlinear equation, the robustness of the shaping algorithm cannot be ensured. The spacecraft and engine's physical parameters (e.g., the initial mass, the thrust magnitude, and the specific impulse) are rarely considered by most of the existing shape-based methods, resulting in that the shape-based trajectory may be infeasible considering the practical constraints.

The aim of this paper is to provide an analytical shaping method by using the cubic spline functions to represent the slow variables of a general 3-D multi-revolution rendezvous trajectory. The idea of shaping the magnitude of the angular momentum is introduced, such that the rendezvous time constraint can be solved analytically. A rapid and robust shaping method is then formulated by suitably designating the segment numbers of cubic spline functions. In addition, by adding free interior points, the optimal control problem is transformed into a parameter optimization problem, where the practical constraints on the spacecraft and engine's parameters can be considered to avoid the infeasible solution. Compared with the existing method [26], the proposed method is superior in terms of the optimality and thrust magnitude, and these characteristics are further improved by the parameter optimization process.

Therefore, the aforementioned problems are satisfactorily overcome by the proposed method. Numerical examples show the superiority of the proposed method, not only in providing an efficient and robust approximation for global search, but also in generating the suitable initial guess for the local optimization.

The rest of this paper is organized as follows. In Sec. 2, the problem of shaping a low-thrust trajectory with parameterized shape functions is introduced, and a parameter optimization problem is then formulated for the corresponding optimal control problem. In Sec. 3, the formulation of shaping trajectory with cubic spline functions is presented, and two types of shaping methods are proposed and compared according to whether they have free optimization parameters. The applications of the proposed trajectory design method are demonstrated by two specific missions in Sec. 4, and Section 5 concludes this paper.

2 Problem Formulation for Shaping Low-Thrust Trajectory

The problem considered here is to approximate the low-thrust trajectory with a near-optimal shape function. The function is intentionally designed to satisfy some constraints, such that a fast estimation for the mission design or an elegant initial guess for the subsequent trajectory optimization can be obtained. It is usually chosen to shape the state vector to avoid the numerical integration of the low-thrust motion equations, and its derivatives are used to analytically evaluate the control law. The general 3-D motion equation for the spacecraft propelled by the low thrust can be formulated as [24]

$$\dot{\mathbf{x}} = \mathbf{A}(\mathbf{x}, t) + \mathbf{B}(\mathbf{x}, t) \mathbf{u} \quad (1)$$

where $\mathbf{x} \in \mathbb{R}^6$ is the state vector, $\mathbf{u} \in \mathbb{R}^3$ is the thrust acceleration, and the expressions of $\mathbf{A} \in \mathbb{R}^6$ and $\mathbf{B} \in \mathbb{R}^{6 \times 3}$ depend on the forces acting on the spacecraft and the considered coordinate system. The 3-D position \mathbf{r} and velocity \mathbf{v} of the spacecraft are given by the state

\mathbf{x} through a transformation from the employed coordinate to the Cartesian coordinate. The thrust acceleration \mathbf{u} is obtained by an inverse transformation of Eq. (1):

$$\mathbf{u} = [\mathbf{B}(\mathbf{x}, t)^T \mathbf{B}(\mathbf{x}, t)]^{-1} \mathbf{B}(\mathbf{x}, t)^T (\dot{\mathbf{x}} - \mathbf{A}(\mathbf{x}, t)) \quad (2)$$

where the state \mathbf{x} and its derivative $\dot{\mathbf{x}}$ are given by the shape function. Based on Eq. (2), the control law \mathbf{u} can always be solved if the thrust is unconstrained, i.e., $\mathbf{B}(\mathbf{x}, t)^T \mathbf{B}(\mathbf{x}, t)$ is invertible [24]. In addition, an implicit condition for a feasible shape trajectory is that the position and velocity given by the shape must satisfy $\dot{\mathbf{r}} = \mathbf{v}$. On this condition, the shape trajectory and the control law can be derived from each other by Eqs. (1) and (2), respectively.

Consider a shape function for the position of the spacecraft $\mathbf{r} = \mathbf{r}(s, \mathbf{z})$, where s is an independent variable nominalized in the interval $[0, 1]$, and \mathbf{z} is the undetermined parameters designed to satisfy constraints. The velocity of spacecraft is then derived as

$$\mathbf{v} = \dot{\mathbf{r}} = \dot{s} \mathbf{r}' \quad (3)$$

where $(*)'$ denotes a derivative with respect to s and $t' = 1 / \dot{s}$ is determined by another shape function $t'(s, \mathbf{z})$. For the low-thrust rendezvous trajectory in a central gravitational field, the motion equation is given by

$$\ddot{s} \mathbf{r}' + \dot{s}^2 \mathbf{r}'' = -\frac{\mu}{r^3} \mathbf{r} + \mathbf{u} \quad (4)$$

where μ is the gravitational parameter of the primary body, $\dot{s} = 1 / t'$, and $\ddot{s} = -t'' / t'^3$. The spacecraft engine has a constant specific impulse I_{sp} and a maximum thrust magnitude T_{max} , therefore the mass of spacecraft is governed by

$$\dot{m} = -\frac{m \|\mathbf{u}\|}{I_{\text{sp}} g_0} \quad (5)$$

where $g_0 = 9.80665 \text{ m/s}^2$ is the standard gravity, while the thrust magnitude for the shape trajectory is constrained:

$$m \|\mathbf{u}\| \leq T_{\text{max}} \quad (6)$$

In addition, the rendezvous boundary states (composed of the initial state $[\mathbf{r}_0^T, \mathbf{v}_0^T]^T$ and the final state $[\mathbf{r}_f^T, \mathbf{v}_f^T]^T$) and the transfer time are both fixed. The corresponding constraints are summarized as follows:

$$\mathbf{r}(0, \mathbf{z}) = \mathbf{r}_0, \quad \mathbf{r}'(0, \mathbf{z}) / t'(0, \mathbf{z}) = \mathbf{v}_0, \quad (7)$$

$$\mathbf{r}(1, \mathbf{z}) = \mathbf{r}_f, \quad \mathbf{r}'(1, \mathbf{z}) / t'(1, \mathbf{z}) = \mathbf{v}_f, \quad (8)$$

$$t_f - t_0 = \int_0^1 t'(s, \mathbf{z}) \, ds \quad (9)$$

where t_0 and t_f denote the initial and final times, respectively. The shape functions incorporating undetermined parameters (i.e., $\mathbf{r}(s, \mathbf{z})$ and $t'(s, \mathbf{z})$) are optimized, such that the corresponding trajectory satisfies the path constraint (6) and boundary constraints (7)–(9). The trajectory can be determined by these functions, while the required thrust acceleration and the spacecraft mass are then obtained from Eqs. (4) and (5), respectively.

Generally, the optimal control problem for the low-thrust trajectory optimization can be transformed into a parameter optimization problem by shaping the trajectory. The performance index for this problem is formulated as

$$J = \phi(\mathbf{z}) + \int_0^1 \varphi(s, \mathbf{z}) \, ds \quad (10)$$

where $\phi(\mathbf{z})$ is the boundary state cost function and $\varphi(s, \mathbf{z})$ is the running cost function [28]. The dynamic constraints are satisfied automatically via Eq. (2), and the path and boundary constraints are collected as Eqs. (6)–(8). Note that the minimum number of the undetermined parameters is equal to the number of equality constraints, that is, 13 in total. In literature, numerous types of functions for $\mathbf{r}(s, \mathbf{z})$ and $t'(s, \mathbf{z})$ are proposed with different number of parameters, e.g., the inverse polynomial in the planar polar coordinate [22], the shape functions in terms of classic or equinoctial elements [26,29], and the Fourier series in the cylindrical coordinate [23]. Instead of shaping the position $\mathbf{r}(s, \mathbf{z})$, Ref. [30] shapes the velocity with some integrable base functions. The independent variable s is usually chosen from the time or

the coordinate parameters, e.g., the polar angle or the true anomaly. Meanwhile, the functions with respect to the time are more complex and usually designed with more optimization parameters [23], whereas the functions with respect to the coordinate parameter result in that the transfer time constraint is nonlinear and its analytical satisfaction is difficult [24].

In this paper, the shape functions in terms of the modified equinoctial orbital elements [31] (MEOEs) $\boldsymbol{\alpha}(s, \mathbf{z}) = [p, f, g, h, k, L]^T$ are formulated. The independent variable is the true longitude given by

$$L = L_0 + s \Delta L \quad (11)$$

where $\Delta L = L_f - L_0$, and L_0 and L_f are the fixed initial and final true longitudes, respectively.

The position of the spacecraft is obtained via the transformation [32]:

$$\mathbf{r} = \frac{r}{\beta^2} \begin{bmatrix} (1 + \alpha^2) \cos L + 2 h k \sin L \\ (1 - \alpha^2) \sin L + 2 h k \cos L \\ 2 (h \sin L - k \cos L) \end{bmatrix} \quad (12)$$

where $r = \|\mathbf{r}\| = p / (1 + f \cos L + g \sin L)$, $\alpha^2 = h^2 - k^2$, and $\beta^2 = 1 + h^2 + k^2$. Then, the velocity and acceleration are derived as

$$\mathbf{v} = \dot{\mathbf{r}} = \frac{d\mathbf{r}}{d\boldsymbol{\alpha}} \dot{\boldsymbol{\alpha}}, \quad (13)$$

$$\mathbf{a} = \dot{\mathbf{v}} = \frac{d\mathbf{r}}{d\boldsymbol{\alpha}} \ddot{\boldsymbol{\alpha}} + \dot{s}^2 \left(\frac{d\mathbf{r}}{d\boldsymbol{\alpha}} \boldsymbol{\alpha}'' + \boldsymbol{\alpha}'^T \frac{d^2\mathbf{r}}{d\boldsymbol{\alpha}^2} \boldsymbol{\alpha}' \right) \quad (14)$$

where the derivatives \dot{s} and \ddot{s} are designated through another shape function for the magnitude of the angular momentum $\dot{h}(s, \mathbf{z}) = r^2 \dot{L}$, viz.

$$\dot{s} = \frac{\dot{L}}{\Delta L} = \frac{\dot{h}}{r^2 \Delta L}, \quad (15)$$

$$\ddot{s} = \frac{\ddot{L}}{\Delta L} = \frac{\dot{s}}{r^2 \Delta L} \left(\dot{h}' - \frac{2 \dot{h} dr}{r d\boldsymbol{\alpha}} \boldsymbol{\alpha}' \right) \quad (16)$$

The detailed expressions for the derivatives $d\mathbf{r}/d\boldsymbol{\alpha}$, $d^2\mathbf{r}/d^2\boldsymbol{\alpha}$, and $dr/d\boldsymbol{\alpha}$ will be given in

the Appendix. Note that the velocity obtained by Eq. (13) may not be equal to the velocity transformed from the MEOEs; that is, these elements shaped here and known as the pseudo-equinoctial elements [24] are not osculating. Finally, a trajectory is designed by the shape function $\boldsymbol{\xi}(s, \mathbf{z}) = [p, f, g, h, k, \hbar]^\top$, whose expressions will be formulated in the next section using cubic spline functions, such that all the boundary constraints could be satisfied analytically.

3 Analytical Shaping with Cubic Spline Functions

In this section, first, the idea of representing the trajectory $\boldsymbol{\xi}(s, \mathbf{z})$ by cubic spline functions is introduced. These functions are second-order continuous, rendering that the velocity and acceleration are both continuous. Then, the constraints on boundary states and transfer time are satisfied by designing the values of boundary and interior points of the cubic spline, respectively. The residual parameters of the cubic spline with multiple segments can be optimized for the satisfaction of some extra constraints (e.g., the thrust magnitude constraint) or better performance index of the trajectory. According to whether there are free optimization parameters, two types of analytical shaping methods are finally proposed, and their computational performance are validated through comparisons to previous studies.

3.1 Analytical Shaping Formulation

Let us decompose the domain of the independent variable s , denoted by S and with the range $[0, 1]$, into n segments such that

$$S = \bigcup_{i=1}^n S_i(s_{i-1}, s_i) \quad (17)$$

where $0 = s_0 < s_1 < \dots < s_n = 1$. At each segment S_i , the function $\boldsymbol{\xi}(s, \mathbf{z})$ is designed as cubic polynomial:

$$\boldsymbol{\xi}(s, \mathbf{z}) = \mathbf{a}_i s^3 + \mathbf{b}_i s^2 + \mathbf{c}_i s + \mathbf{d}_i, \quad s \in S_i \quad (18)$$

where the vectors \mathbf{a}_i , \mathbf{b}_i , \mathbf{c}_i , and \mathbf{d}_i are the coefficients to be settled. Since the position and velocity of the spacecraft must be continuous, the shaping elements $\boldsymbol{\alpha}$, its derivative $\boldsymbol{\alpha}'$, and the magnitude of the angular momentum \hbar are all continuous (see Eqs. (12) and (13)). Besides, the acceleration is usually discontinuous in practice, while it is herein assumed to be continuous to approximate the low-thrust trajectory [22]. Thus, the function $\hbar(s, \mathbf{z})$ should be first-order continuous, and the others are second-order continuous. In order to use a uniform formulation, the function $\boldsymbol{\xi}(s, \mathbf{z})$ is designed with second-order continuity ($\boldsymbol{\xi}(s, \mathbf{z}) \in C^2[0, 1]$); that is, it is a cubic spline function. In this case, the undetermined parameter \mathbf{z} consists of the values of $\boldsymbol{\xi}(s_i)$, $i = 0, 1, \dots, n$ and two additional boundary conditions of the cubic spline, which are usually set according to the first or second order derivatives to $\boldsymbol{\xi}$ [33]. The other conditions used to settle the coefficients are derived from the aforesaid continuations between adjacent segments, such that the number of conditions is the same as the number of unknown coefficients.

To determine the cubic spline functions, the following boundary conditions are considered:

$$\boldsymbol{\xi}'(0) = 0, \quad \boldsymbol{\xi}'(1) = 0 \quad (19)$$

By substituting Eqs. (15) and (19) into Eq. (13), the velocity takes the same form as that of the osculating orbital elements, i.e., $\mathbf{v} = \dot{L} d\mathbf{r}/dL$. Thus, the shape orbital elements at boundary points are osculating, and the boundary conditions of rendezvous are satisfied by setting the values of the boundary shape functions with the boundary osculating orbital elements and angular momentum magnitudes, viz.

$$\boldsymbol{\xi}(0) = [p_0, f_0, g_0, h_0, k_0, \hbar_0]^T, \quad (20)$$

$$\boldsymbol{\xi}(1) = [p_f, f_f, g_f, h_f, k_f, \hbar_f]^T \quad (21)$$

The other variables are $\xi(s_i)$, $i = 1, 2, \dots, n-1$ at the interior points. Meanwhile, the value of semi-latus rectum at the first interior point p_1 is designated to satisfy the transfer time constraint, while the other variables are free optimization parameters that need to be optimized. For a given final time t_f , the transfer time constraint is

$$\int_0^1 \frac{p^2 \Delta L}{\hbar (1 + f \cos L + g \sin L)^2} ds + t_0 - t_f = 0 \quad (22)$$

Note that the shape function $p(s)$ is proportional to p_1 according to the cubic spline formulation, viz.

$$p(s) = \gamma_1(s) p_1 + \gamma_2(s) \quad (23)$$

Then, taking the parameter p_1 as the unknown variable, we can integrated Eq. (22) as

$$a_t p_1^2 + b_t p_1 + c_t = 0 \quad (24)$$

where the coefficients are

$$a_t = \int_0^1 \frac{\gamma_1^2 \Delta L}{\hbar (1 + f \cos L + g \sin L)^2} ds > 0, \quad (25)$$

$$b_t = \int_0^1 \frac{2 \gamma_1 \gamma_2 \Delta L}{\hbar (1 + f \cos L + g \sin L)^2} ds, \quad (26)$$

$$c_t = \int_0^1 \frac{\gamma_2^2 \Delta L}{\hbar (1 + f \cos L + g \sin L)^2} ds + t_0 - t_f \quad (27)$$

The free optimization parameters are solved by a direct optimization algorithm, and these coefficients can be integrated rapidly via quadrature using the trapezoidal rule [22]. There are two values for p_1 :

$$p_1^{(1)} = \frac{-b_t + \sqrt{b_t^2 - 4 a_t c_t}}{2 a_t}, \quad p_1^{(2)} = \frac{-b_t - \sqrt{b_t^2 - 4 a_t c_t}}{2 a_t} \quad (28)$$

Because $a_t > 0$, the discriminant $\Delta_t = b_t^2 - 4 a_t c_t$ is an increasing function with respect to the transfer time $t_f - t_0$. The first solution $p_1^{(1)}$ is also an increasing function of transfer time, while the second one $p_1^{(2)}$ is a decreasing function. After setting the optimization parameters, there may be no feasible solution (i.e., $\Delta_t < 0$) when the transfer time is too short. In addition, the

semi-latus rectum p_1 is checked posteriorly to guarantee its value larger than a given minimum value $p_{1\min}$. Thus, the following condition for shaping a feasible trajectory is obtained:

$$\Delta_t \geq 0 \wedge \Delta_p = \max \{p_1^{(1)}, p_1^{(2)}\} - p_{1\min} \geq 0 \quad (29)$$

If this condition is violated, p_1 is set to p_0 in the simulation, and the resulting transfer time cannot satisfy its constraint. Later on, this infeasible solution will be avoided by adding the penalty functions to the performance index. If the two solutions are both feasible, the solution with better performance index is preferred. Note that the first one is more consistent with our trajectory design experience because $p_1^{(1)}$ increases over the transfer time.

By designating the aforesaid 13 variables $\boldsymbol{\xi}(0)$, $\boldsymbol{\xi}(1)$, and p_1 to satisfy the analytical boundary equality constraints, the free parameters become $\{\boldsymbol{\xi}(s_i), i = 1, 2, \dots, n-1\} \setminus \{p_1\}$. The optimization problem is now to minimize the performance index Eq. (10) subject to the path constraint Eq. (6). In this study, the propellant consumption integrated by Eq. (5) is regarded as the performance index:

$$J = m_0 \left[1 - \exp \left(-\frac{1}{I_{sp} g_0} \int_0^1 \|\mathbf{u}\| ds \right) \right] - \rho_1 \min \{\Delta_t, 0\} - \rho_2 \min \{\Delta_p, 0\} \quad (30)$$

where \exp is the exponential function, and ρ_1 and ρ_2 are penalty functions for those solutions violating Eq. (29). In numerical simulation, setting $\rho_1 = \rho_2 = 1 \times 10^4$ is adequate to avoid the infeasible trajectory. Noted that another equivalent choice is to minimize the total velocity increment $\Delta V = \int_0^1 \|\mathbf{u}\| ds$, which is independent of the spacecraft and engine's parameters. Thus, the influence of these parameters on the optimal solution is not reflected in the performance index but included in the path constraint.

3.2 Shaping Methods for 3-D Orbital Rendezvous

The shape functions for different shaping elements can employ different number of segments; that is, $\mathbf{n} = [n_p, n_f, n_g, n_h, n_k, n_h]^T$. The number of segments for the semi-latus rectum n_p must be larger than 2 for the rendezvous trajectory, while the minimum values for the others are 1. Thus, the total number of free parameters is $\|\mathbf{n}\|_1 - 7$. In this subsection, two types of shaping methods with different segment numbers are formulated according to whether they have free optimization parameters. The first one is to shape the rendezvous trajectory rapidly by setting $n_p = 2$ and $n_f = n_g = n_h = n_k = n_h = 1$, where the thrust magnitude constraint is not considered. The second one is to shape the trajectory with thrust magnitude constraint by setting $n_p = n_f = n_g = n_h = n_k = n_h = n \geq 2$. For the two shaping methods investigated here, the segment intervals of each group of shaping elements are assumed to be equal:

$$s_i - s_{i-1} = 1/n, \quad i = 1, 2, \dots, n \quad (31)$$

3.2.1 Rapid shaping method neglecting thrust magnitude constraint

Let $n_p = 2$ and $n_f = n_g = n_h = n_k = n_h = 1$, and the rendezvous trajectory is shaped by the corresponding functions. A two-segment piecewise cubic polynomial is formulated for the semi-latus rectum:

$$p = \begin{cases} p_0 + 3(p_f - p_0) s^2 - 2(p_f - p_0) s^3 + 4(3s^2 - 4s^3) \Delta p, & \text{if } s \leq 0.5 \\ p_0 + 3(p_f - p_0) s^2 - 2(p_f - p_0) s^3 - 4(1 - 6s + 9s^2 - 4s^3) \Delta p, & \text{if } s > 0.5 \end{cases} \quad (32)$$

where $\Delta p \triangleq p_1 - (p_f - p_0)/2$. The other elements are also shaped by cubic polynomials:

$$f = f_0 + 3(f_f - f_0) s^2 - 2(f_f - f_0) s^3 \quad (33)$$

$$g = g_0 + 3(g_f - g_0) s^2 - 2(g_f - g_0) s^3 \quad (34)$$

$$h = h_0 + 3(h_f - h_0) s^2 - 2(h_f - h_0) s^3 \quad (35)$$

$$k = k_0 + 3(k_f - k_0) s^2 - 2(k_f - k_0) s^3 \quad (36)$$

$$\hbar = \hbar_0 + 3(\hbar_f - \hbar_0) s^2 - 2(\hbar_f - \hbar_0) s^3 \quad (37)$$

All the boundary constraints discussed in the previous subsection are satisfied by substituting Eqs. (32)–(37) into Eqs. (19)–(22). To simplify the formulation for the semi-latus rectum, Δp is designed to meet the transfer time constraint. A quadratic equation can be obtained and solved similarly to Eq. (24). When the value of Δp is zero, the piecewise formulation becomes a cubic polynomial function. The integral of Eq. (22) can be obtained analytically when the rendezvous trajectory between circular orbits is considered. However, for the general cases of rendezvous trajectories with multiple revolutions and large out-of-plane motions, the trapezoidal rule is employed to integrate the transfer time.

3.2.2 Shaping method with thrust magnitude constraint

By setting $n_p = n_f = n_g = n_h = n_k = n_{\hbar} = n \geq 2$ and optimizing the free parameters $\{\xi(s_i), i = 1, 2, \dots, n-1\} \setminus \{p_1\}$, the shape functions can be formulated through a standard cubic spline interpolation algorithm. In this case, it is difficult to give the explicit expressions of $\gamma_1(s)$ and $\gamma_2(s)$. To obtain the coefficients of the quartic equation for the transfer time, three values of $\Delta p \triangleq p_1 - (p_0 + p_2)/2$ are tested, i.e., $\Delta p_1 = (p_2 - p_0)/2$, $\Delta p_2 = -\Delta p_1$, and $\Delta p_3 = 0$. Their transfer times are denoted by t_1 , t_2 , and t_3 , respectively. Then, the coefficients are obtained as

$$c_t = t_3 + t_0 - t_f, \quad b_t = \frac{t_1 - t_2}{2 \Delta p_1}, \quad a_t = \frac{t_1 + t_2 - 2t_3}{2 \Delta p_1^2} \quad (38)$$

Instead of Eqs. (25)–(27), the above equations are utilized to solve the exact Δp that satisfies the transfer time constraint.

The thrust magnitude constraint is considered at some discrete points, viz,

$$m(s_{ij}) \|\mathbf{u}(s_{ij})\| \leq T_{\max}, \quad j = 0, 1, \dots, c \quad (39)$$

where $s_{i-1} = s_{i0} < s_{i1} < \dots < s_{ic} = s_i$, $i = 1, 2, \dots, n$, and c is the number of discrete points of segment S_i . The number $c \geq 1$ is set to the same value for every segment because their intervals are equal. Assuming that these discrete points are also equally spaced, the value of independent variable at each point is

$$s_{ij} = \frac{1}{n} \left(i - 1 + \frac{j}{c} \right), \quad i = 1, 2, \dots, n; \quad j = 0, 1, \dots, c \quad (40)$$

Since the boundary points of adjacent segments are counted twice, the total number of constrained points is $nc + 1$. After setting the values of n and c , a parameter optimization algorithm is utilized to find the propellant-optimal solution with thrust magnitude constraint.

3.3 Computational Comparisons to Previous Studies

To verify the proposed shaping methods, this subsection presents a rendezvous example, in which the initial and target orbital elements in the heliocentric ecliptic J2000 frame are set to compare the results with those of Ref. [26]. As shown in Table 1, a general 3-D rendezvous between elliptic orbits is performed. The spacecraft departs from the initial orbit at $t_0 = 0$ and arrives the target orbit at t_f . The astronomical unit is set to $1 \text{ AU} = 149597870.7 \text{ km}$, and the gravitational parameter of the Sun is $\mu = 132712440018 \text{ km}^3/\text{s}^2$.

The results of the shape trajectories neglecting the thrust magnitude constraint are firstly presented. As stated before, the trajectory is independent of the parameters of spacecraft and engine, and these parameters will be chosen later on for the shaping method with thrust magnitude constraint. The rendezvous trajectories are shaped with a series of transfer times $t_f = 8, 16, 24, 32, 40$, and 48 years, in which multiple revolutions are usually employed. The

Table 1

Initial and target classic orbital elements [26]

Orbits	a , AU	e	i , deg	Ω , deg	ω , deg	f , deg
Initial	1.0	0.4	10.0	15.0	25.0	10.0
Target	3.0	0.6	40.0	25.0	25.0	40.0

optimal revolution numbers that yield the minimum velocity increments are obtained, and the corresponding velocity increments ΔV and maximum thrust accelerations u_{\max} during the rendezvous are compared in Table 2. It shows that the rendezvous trajectories generated by the proposed method take smaller velocity increments and thrust accelerations. The computational results of the proposed method are more superior than the previous results for all test cases. The computational efficiency will be demonstrated later on in Sec. 4.1. As the transfer time increases, the trajectory needs more revolution number, larger velocity increment, and smaller thrust acceleration.

The rendezvous case with $t_f = 16$ years is then tested to demonstrate the effectiveness of the proposed shaping method with the thrust magnitude constraint. The spacecraft is assumed to have an initial mass $m_0 = 4000$ kg, a constant specific impulse $I_{\text{sp}} = 3000$ s, and a maximum thrust magnitude $T_{\max} = 0.6$ N. The initial thrust acceleration is $T_{\max}/m_0 = 0.15$ mm/s², which is admittedly smaller than the obtained result $u_{\max} = 0.8$ mm/s² (shown in Table 2). The Powell's COBYLA algorithm [34] in the NLOpt library is used for the parameter optimization, where the relative tolerance is set to 10^{-4} . The first guesses for the free parameters are generated by the rapid shaping results. The computational results with different numbers of segments and discrete points are listed in Table 3. It is shown that better performance is obtained as the segment number increases. The thrust magnitude constraint is more strictly satisfied when more discrete points are set, and the corresponding performance index becomes worse in general. It is a trade-off between the performance index and the thrust magnitude

Table 2

Comparisons of rendezvous results with different transfer times

t_f , years	Proposed Shaping Method			Shaping Method in Ref. [26]		
	N_{opt}	ΔV , km/s	u_{max} , mm/s ²	N_{opt}	ΔV , km/s	u_{max} , mm/s ²
8	3	23.01	1.22	3	27.77	2.41
16	6	22.66	0.64	5	31.25	1.74
24	9	23.29	0.44	7	34.66	1.35
32	12	24.69	0.35	9	38.91	1.17
40	15	26.67	0.29	11	43.64	1.09
48	18	29.07	0.25	12	48.23	0.97

constraint. Nevertheless, all results obtained here are better than the results shown in Table 2, but at the cost of more computational time for the parameter optimization. Note that the COBYLA algorithm uses a linear approximation to the constraints and performance index, whose computational efficiency is admittedly poor for the nonlinear optimization problem. As shown in Table 3, the optimization takes a few minutes to obtain the rendezvous trajectories with the thrust magnitude constraint. Thus, to achieve fast estimation, the analytical shaping method neglecting the thrust magnitude constraint or optimization with larger relative tolerance is suggested.

The proposed shaping method shows its effectiveness in providing fast and accurate estimation for the preliminary mission design. Compared with the results reported in Ref. [26], the results generated by the proposed method have better performance, and the efficiency and robustness of shaping are improved because no Newtonian iterative process is required. In addition, the proposed shaping method may not achieve the optimal solution even it uses many segments,

Table 3

Comparisons of rendezvous results with thrust magnitude constraint

Solution	n	c	T_{\max} , N	ΔV , km/s	m_f , kg	CPU time, min
1	10	5	0.73135	20.72	1978.06	3.84
2	10	10	0.60836	20.90	1966.08	4.10
3	15	5	0.61826	17.24	2225.97	11.40
4	15	10	0.60734	17.35	2217.75	5.25
5	20	5	0.60687	16.28	2299.92	10.99
6	20	10	0.60193	16.27	2300.62	10.83

due to the subjective assumptions of second-order continuity and zero boundary conditions (see Eq. (19)). Thus, to find the optimal trajectory, we should use the proposed method to find good initial guesses and then turn to the traditional direct or indirect methods [2,35,36,37].

4 Applications to Trajectory Design

The shaping method has been widely used to approximate the low-thrust transfer, rendezvous, and gravity-assist trajectories in combination with the global search algorithms [22,25]. However, the performance of trajectory design is highly dependent on the estimation accuracy of the shape functions. For the 3-D multi-revolution rendezvous trajectories, the applications of proposed shaping method are presented in this section through two mission scenarios, a rendezvous mission from the Earth to asteroid Dionysus [38] and a Near-Earth Asteroids sample return mission [10]. The epochs of these two missions are designed by using the proposed shaping method for estimation and the particle swarm optimization (PSO) method [39] for global

search. To achieve the fast estimation, the proposed shaping method neglecting the thrust magnitude constraint is employed here. Two other estimation methods are compared: 1) the impulsive solution to the Lambert problem [10]; 2) the shaping method reported in Ref. [26]. Based on the PSO search results, the final propellant-optimal trajectories for the two missions are solved by the indirect method. The performance of the proposed method in initial guessing is presented with comparison to the results in Ref. [13].

Table 4

Classic orbital elements of the Earth and targets (56000 MJD)

Name	a , AU	e	i , deg	Ω , deg	ω , deg	f , deg
Earth	0.999584	0.016375	0.002666	134.239190	329.982886	69.425162
Dionysus	2.199238	0.541127	13.526692	82.074057	204.296334	180.509774
1999 AO ₁₀	0.911569	0.110968	2.624497	313.313332	7.678286	186.819009
2000 LG ₆	0.917259	0.110893	2.830149	72.571729	8.144765	312.238767

4.1 Rendezvous with Dionysus

Consider a multi-revolution rendezvous mission, in which the spacecraft departs from the Earth to rendezvous with the asteroid Dionysus. The orbital elements of the Earth and Dionysus are listed in Table 4. The spacecraft is assumed to have a constant specific impulse $I_{\text{sp}} = 3000$ s, a maximum thrust magnitude $T_{\text{max}} = 0.32$ N, and an initial mass $m_0 = 4000$ kg. The launch epoch t_0 is chosen in $t_0 \in [56000, 56500]$ MJD, and the arrival epoch t_f is in $t_f \in [59000, 60000]$ MJD. Then, the PSO algorithm is used to optimize the launch and arrival epochs. Because multiple revolutions are needed, the optimal revolution numbers that take the minimum propellant consumption are chosen identically for all the estimation methods.

The results of epochs are collected in Table 5. The maximal iteration number for the PSO algorithm is set to $n_{\max} = 100$, and the swarm size is set to $S = 20$. The simulation programs are written in C++, compiled with Microsoft Visual Studio 2012 using the release mode and single thread, and run on a desktop computer with an Intel Core i7-7700 CPU of 3.6 GHz and 8.00 GB of RAM. Because the Lambert problem uses two impulsive maneuvers to perform the rendezvous, its estimated propellant consumption is smallest. The solving of the Lambert problem is much faster than the other methods. After the first impulse is applied, the spacecraft enters a transfer orbit, and the value of its semi-major axis is between those of the initial and target orbits. Thus, the revolution number of the Lambert solution is fewest but infeasible for a continuous low thrust. Compared with the shaping method in Ref. [26], the proposed method shows its effectiveness in smaller propellant consumption (2006.6 kg v.s. 2596.4 kg) and shorter CPU time (12.2 s v.s. 182.8 s).

Table 5

Results of epochs by the PSO search

Estimation Method	t_0 , MJD	t_f , MJD	N_{opt}	Δm , kg	CPU time, s
Lambert Solution	56483.082	59299.275	2	1179.047	0.1
Shaping Method [26]	56363.610	59000.078	4	2596.365	182.8
Proposed Method	56329.586	59872.983	5	2006.622	12.2

The launch and arrival epochs are determined by the PSO search results, and the indirect method [40] is then employed to solve the corresponding propellant-optimal solutions. The techniques of the energy-propellant homotopy, costates normalization, and random guess strategy presented in Ref. [40] are applied here and their details are omitted here for brevity. The propellant-optimal results are listed in Table 6, where the epochs keep the same values as those in Table 5. It shows that both the shaping method [26] and proposed method provide good estimations to the revolution numbers. The optimal solution is $\Delta m_{\text{opt}} = 1279.93$ kg, in which

the epochs are searched by the proposed method. Thus, the proposed method is superior in identifying the optimal epochs for the preliminary design.

Table 6

Propellant-optimal results for different epochs

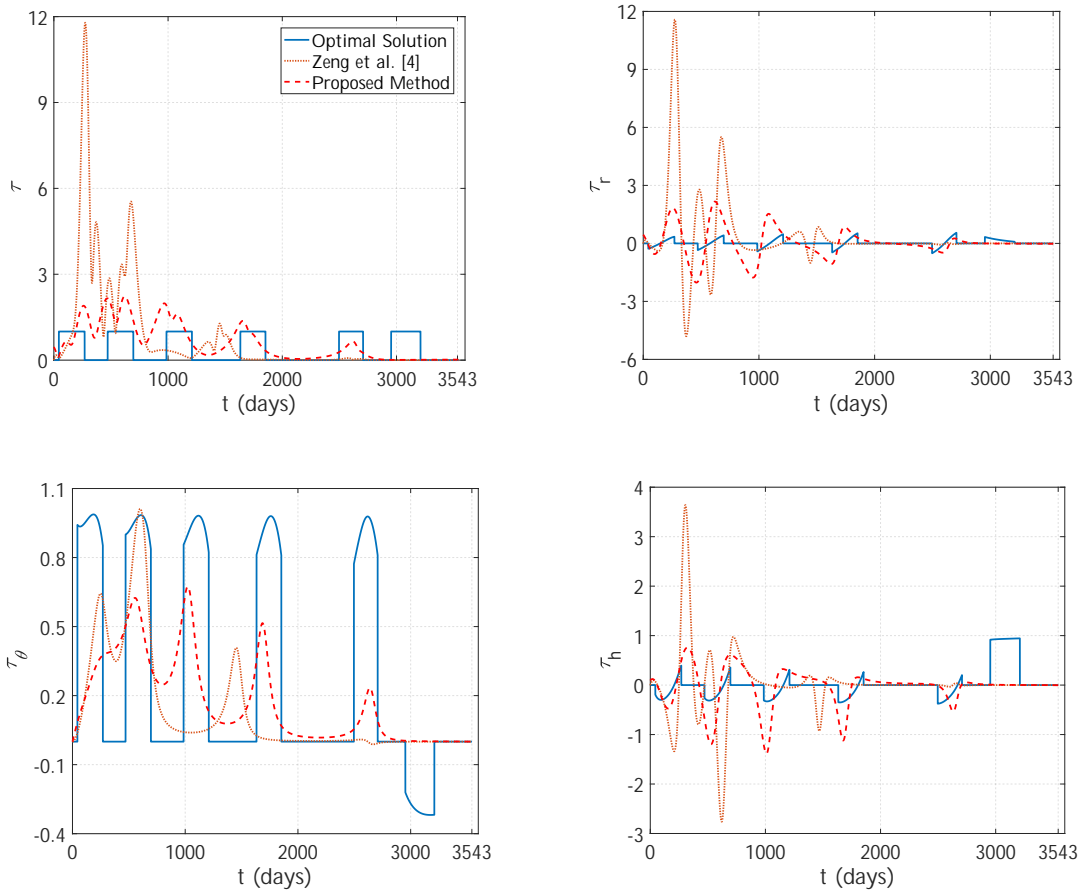
Solution	t_0 , MJD	t_f , MJD	N_{opt}	Δm_{opt} , kg
1	56483.082	59299.275	5	1390.679
2	56363.610	59000.078	4	1370.658
3	56329.586	59872.983	5	1279.930

In addition, the solution 3 is investigated to demonstrate the effectiveness of the proposed method in providing initial guesses. The costates estimation technique [13] around a shaping trajectory is used here for the energy-optimal problem, and a energy-propellant homotopy process is subsequently employed to obtain the optimal solution. For comparison, three strategies are tested: 1) random guess with the costate normalization [40]; 2) costates estimation in combination with the shaping method in Ref. [26]; 3) costates estimation using the proposed method. The initial costates and the percentage of converged (POC) cases out of 1000 run are summarized in Table 7. The proposed method improves the estimation POC to 51.4%, higher than the other results, and the average computational time (ACT) for one solution reduces from 12.2 s to 1.4 s. Furthermore, as reported in Ref. [13], the performance of costates estimation relies on the assumption that the shaping trajectory is generally close to the optimal one. The profiles of the thrust components, propellant consumptions, and the trajectories of different methods are collected in Figs. 1–3, respectively. They show that the proposed method provides better estimations to the control and state variables.

Table 7

Results of energy-optimal problem by costates estimation

Initial Guesses	Values of initial costates using MEOEs	POC, %	ACT, s
Random Guess [13]	-	6.4	12.2
Shaping method [26]	$[-0.8359, -0.3604, 1.3840, -0.3632, -0.4956, 0.0137, 0.5]$	11.2	9.4
Proposed method	$[-0.5598, -0.2260, 0.8556, -0.3998, -0.6346, 0.0067, 0.5]$	51.4	1.4
Energy Optimal	$[-0.3580, -0.0319, 0.1597, -0.1689, -0.3359, 0.0006, 0.4]$	-	-

Fig. 1. Profiles of thrust components for different methods ($\tau = \mathbf{u} / T_{\max}$).

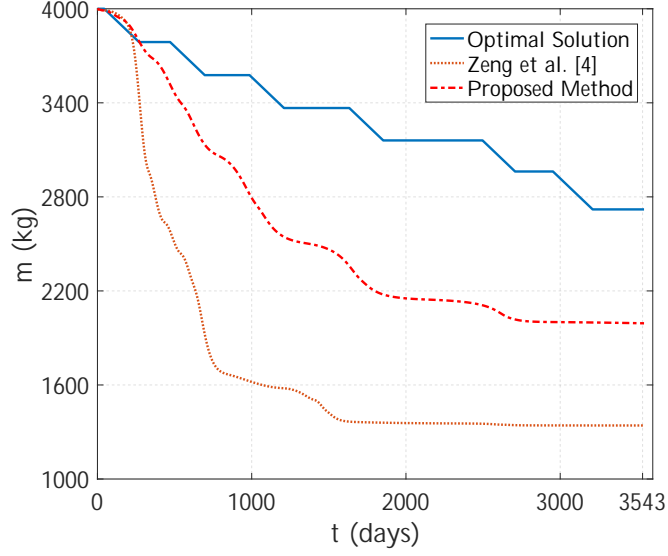


Fig. 2. Histories of the spacecraft mass

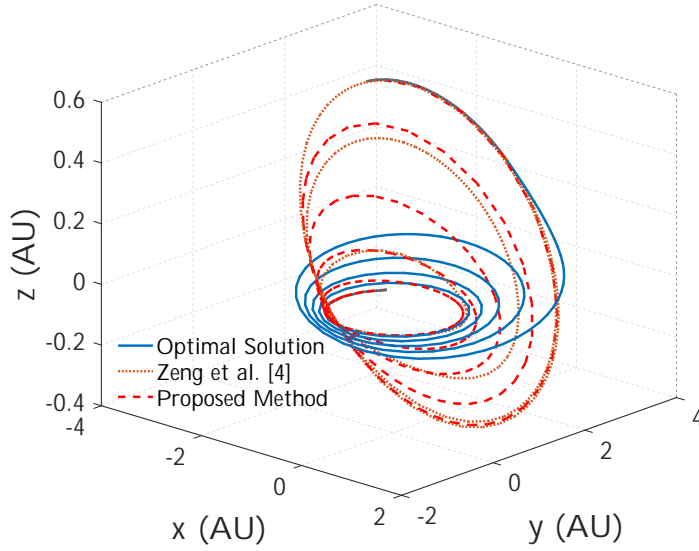


Fig. 3. 3-D trajectories for different methods.

4.2 Near-Earth Asteroids Sample Return

A sample return mission with multiple targets is studied in this subsection to design the multi-rendezvous low-thrust trajectory. The orbital elements of the Earth and targets are also given in Table 4. The spacecraft is assumed to have a constant specific impulse $I_{sp} = 3000$ s, a maximum thrust magnitude $T_{max} = 0.36$ N, and an initial mass $m_0 = 1500$ kg. The sequential

rendezvous with 1999 AO₁₀, 2000 LG₆, and the Earth are considered in this mission [10]. After rendezvous with a target asteroid, the spacecraft takes 60 days to carry out sampling tasks, while the sampling mass is negligible compared with the spacecraft mass. Based on the preliminary design results introduced in Ref. [10], the epochs when the spacecraft departs from the Earth and arrives at each targets are re-optimized here by the PSO search in combination with the proposed estimation method.

As shown in Table 8, the results obtained by using the shaping method [26] and the proposed method are searched in the range of $\Delta t \in [-300, 300]$ days, subjected to the corresponding preliminary design results of the Lambert solution [10]. For each method, two optimal results are obtained by the indirect method, including the optimal single-leg rendezvous solution where all the epochs are fixed at the results of PSO search and the multi-leg rendezvous solution where the interior epochs are free. Thus, the propellant consumption of the second one is less. Note that the results corresponding to the Lambert solution are different from those reported in Ref. [10] because they are different local optimal solutions. The new results obtained here have less propellant consumption. The propellant consumptions of solutions 5 and 6 are close to each other and less than others. Table 8 clearly shows the superiority of the proposed method in searching for the globally optimal solution.

Furthermore, the optimal solution of the multi-rendezvous mission takes $\Delta m_{\text{opt}} = 442.20$ kg in total. The spacecraft firstly departs from the Earth at 63309.826 MJD to rendezvous with the 1999 AO₁₀ in $\Delta t_1 = 587.549$ days with a propellant consumption $\Delta m_1 = 128.64$ kg. Then, the second leg from the 1999 AO₁₀ to 2000 LG₆ takes $\Delta t_2 = 809.080$ days and $\Delta m_2 = 234.19$ kg. Finally, the spacecraft returns to the Earth with another $\Delta t_3 = 570.709$ days and $\Delta m_3 = 79.37$ kg. The histories of the thrust magnitude and spacecraft mass are plotted in Figs. 4 and 5, respectively. The structure of bang-bang control is obtained, in which several burn arcs are very short (the lengths of the three shortest arcs are all less than 8 days). The propellant-optimal rendezvous trajectories are plotted in Figs. 6–8. The spacecraft arrives at the 1999

Table 8

Results for the multi-rendezvous mission

Estimation Method	Solution	Values of epochs	Δm_{opt} , kg
Lambert Solution [10]	1	[63608.374, 63960.859, 64752.511, 65336.956]	497.41
	2	[63608.374, 63971.934, 64764.218, 65336.956]	490.42
Shaping method [26]	3	[63451.125, 64135.812, 64725.645, 65420.367]	616.34
	4	[63451.125, 63948.783, 64767.835, 65420.367]	451.34
Proposed method	5	[63309.826, 63897.212, 64762.270, 65337.164]	442.64
	6	[63309.826, 63897.375, 64766.455, 65337.164]	442.20

AO₁₀ and Earth earlier than the given rendezvous epochs, implying that this solution can be further improved by adjusting the launch and return epochs.

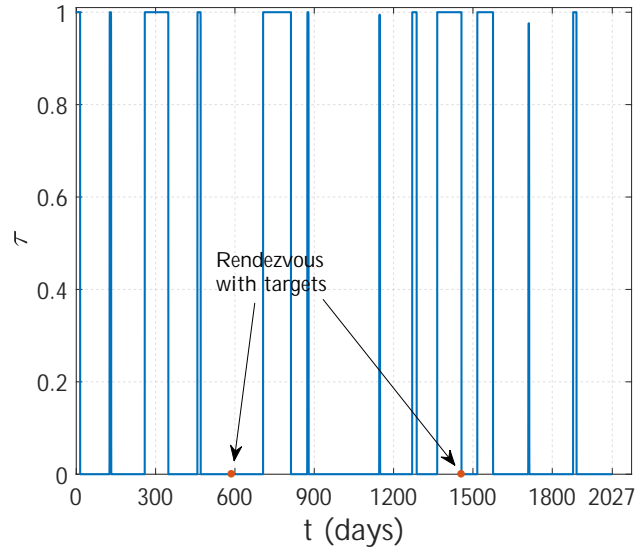


Fig. 4. Thrust magnitude for the multi-rendezvous mission (solution 6).

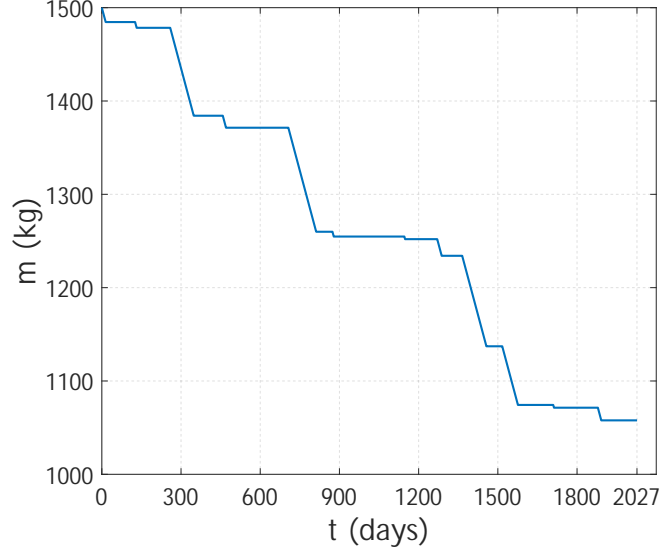


Fig. 5. Histories of the spacecraft mass for the multi-rendezvous mission.

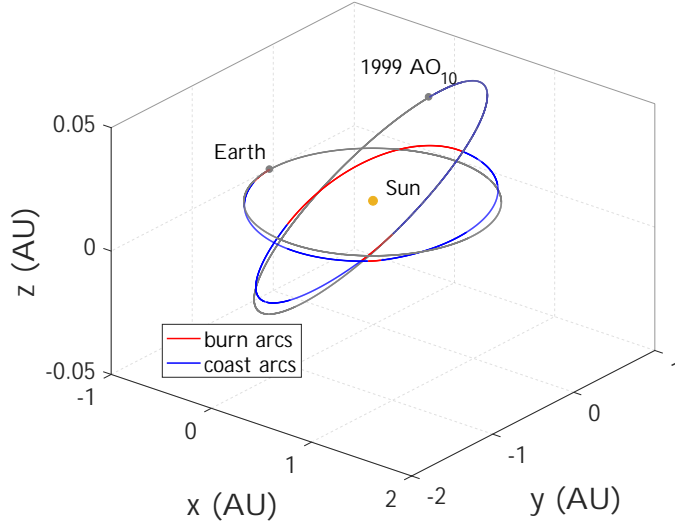


Fig. 6. Propellant-optimal trajectory from Earth to 1999 AO₁₀.

5 Conclusions

In this paper, an analytical shaping method is proposed to approximate the general 3-D multi-revolution low-thrust rendezvous trajectory using the cubic spline functions. The boundary constraints are all analytically satisfied with the parameters of the shape function. When neglecting the thrust magnitude constraint, the Newtonian iterative process is no longer needed,

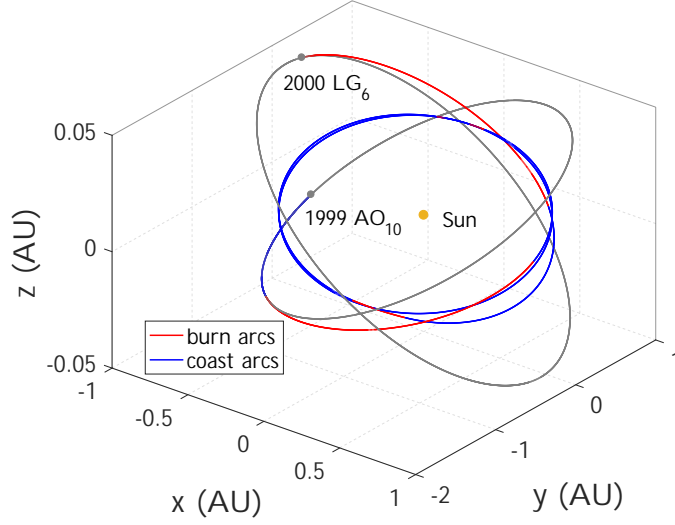


Fig. 7. Propellant-optimal trajectory from 1999 AO₁₀ to 2000 LG₆.

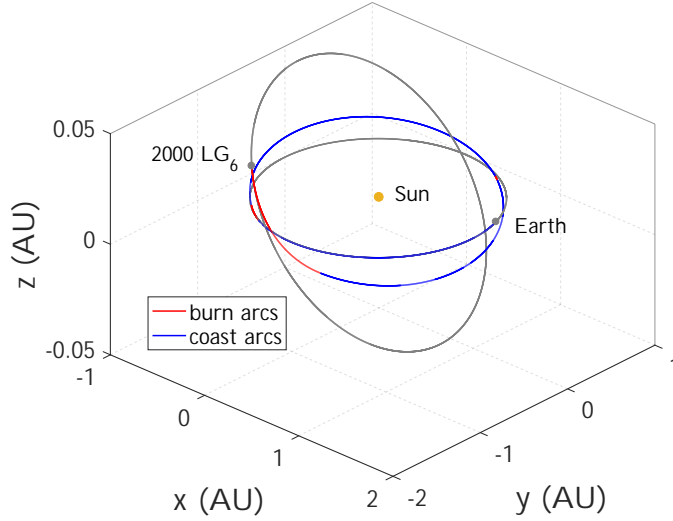


Fig. 8. Propellant-optimal trajectory from 2000 LG₆ to Earth.

and a fast and robust shaping algorithm is achieved. Moreover, a parameter optimization problem with several discrete segments and constrained points is formulated and solved to provide better approximation results considering the constraints on the physical parameters of the spacecraft and its engine.

Compared with the existing 3-D shaping method, the proposed method shows remarkable advantages both in the less total velocity increment and smaller maximum acceleration. The effectiveness and robustness of the proposed method are demonstrated via a multi-revolution

interplanetary rendezvous mission and a multi-rendezvous sample return mission. The proposed method provides good estimations for the global search and improves the convergence percentage of the initial guesses for the indirect method.

6 Acknowledgment

This work was supported by the National Natural Science Foundation of China (grant nos. 12022214).

Appendix: Expressions for $d\mathbf{r}/d\boldsymbol{\alpha}$, $d\mathbf{r}^2/d^2\boldsymbol{\alpha}$, and $d\mathbf{r}/d\boldsymbol{\alpha}$

In this section, the derivatives in terms of the MEOEs for the shaping approximation are presented. For clarity, the following parameters are defined:

$$\eta_1 = 1 + f \cos L + g \sin L, \quad \eta_2 = (f \sin L - g \cos L) / \eta_1, \quad \eta_3 = (f \cos L + g \sin L) / \eta_1,$$

$$\eta_4 = h \sin L - k \cos L, \quad \eta_5 = h \cos L + k \sin L, \quad \eta_6 = h \cos L - k \sin L,$$

$$\eta_7 = \sin L - \eta_2 \cos L, \quad \eta_8 = \cos L + \eta_2 \sin L, \quad \eta_9 = 2\eta_2^2 + \eta_3 - 1$$

According to Eq. (12), the derivatives $d\mathbf{r}/d\boldsymbol{\alpha}$ are obtained

$$\frac{\partial \mathbf{r}}{\partial p} = \frac{\mathbf{r}}{p}, \quad \frac{\partial \mathbf{r}}{\partial f} = -\frac{\mathbf{r} \cos L}{\eta_1}, \quad \frac{\partial \mathbf{r}}{\partial g} = -\frac{\mathbf{r} \sin L}{\eta_1},$$

$$\frac{\partial \mathbf{r}}{\partial h} = -\frac{2\mathbf{r}h}{\beta^2} + \frac{2r}{\beta^2} [\eta_5, -\eta_4, \sin L]^T, \quad \frac{\partial \mathbf{r}}{\partial k} = -\frac{2\mathbf{r}k}{\beta^2} + \frac{2r}{\beta^2} [\eta_4, \eta_5, -\cos L]^T,$$

$$\frac{\partial \mathbf{r}}{\partial L} = \eta_2 \mathbf{r} + \frac{r}{\beta^2} [2hk \cos L - (1 + \alpha^2) \sin L, (1 - \alpha^2) \cos L - 2hk \sin L, 2\eta_5]^T$$

Then, the derivatives $d\mathbf{r}^2/d^2\boldsymbol{\alpha}$ are derived as

$$\begin{aligned}
\frac{\partial^2 \mathbf{r}}{\partial p^2} &= 0, \quad \frac{\partial^2 \mathbf{r}}{\partial p \partial f} = \frac{\partial \mathbf{r}}{p \partial f}, \quad \frac{\partial^2 \mathbf{r}}{\partial p \partial g} = \frac{\partial \mathbf{r}}{p \partial g}, \quad \frac{\partial^2 \mathbf{r}}{\partial p \partial h} = \frac{\partial \mathbf{r}}{p \partial h}, \quad \frac{\partial^2 \mathbf{r}}{\partial p \partial k} = \frac{\partial \mathbf{r}}{p \partial k}, \quad \frac{\partial^2 \mathbf{r}}{\partial p \partial L} = \frac{\partial \mathbf{r}}{p \partial L}, \\
\frac{\partial^2 \mathbf{r}}{\partial f^2} &= \frac{2 \mathbf{r} \cos^2 L}{\eta_1^2}, \quad \frac{\partial^2 \mathbf{r}}{\partial h^2} = \frac{8 h^2 \mathbf{r}}{\beta^4} - \frac{4 r}{\beta^4} [2 h \eta_5 + k \eta_4, \sin L + k \eta_5 - 2 h \eta_4, 2 h \sin L + \eta_4]^T, \\
\frac{\partial^2 \mathbf{r}}{\partial g^2} &= \frac{2 \mathbf{r} \sin^2 L}{\eta_1^2}, \quad \frac{\partial^2 \mathbf{r}}{\partial k^2} = \frac{8 k^2 \mathbf{r}}{\beta^4} - \frac{4 r}{\beta^4} [\cos L + h \eta_5 + 2 k \eta_4, 2 k \eta_5 - h \eta_4, \eta_4 - 2 k \cos L]^T, \\
\frac{\partial^2 \mathbf{r}}{\partial L^2} &= \eta_9 \mathbf{r} + \frac{2 r \eta_2}{\beta^2} [2 h k \cos L - (1 + \alpha^2) \sin L, (1 - \alpha^2) \cos L - 2 h k \sin L, 2 \eta_5]^T, \\
\frac{\partial^2 \mathbf{r}}{\partial f \partial h} &= -\frac{\cos L}{\eta_1} \frac{\partial \mathbf{r}}{\partial h}, \quad \frac{\partial^2 \mathbf{r}}{\partial f \partial k} = -\frac{\cos L}{\eta_1} \frac{\partial \mathbf{r}}{\partial k}, \quad \frac{\partial^2 \mathbf{r}}{\partial g \partial h} = -\frac{\sin L}{\eta_1} \frac{\partial \mathbf{r}}{\partial h}, \quad \frac{\partial^2 \mathbf{r}}{\partial g \partial k} = -\frac{\sin L}{\eta_1} \frac{\partial \mathbf{r}}{\partial k}, \\
\frac{\partial^2 \mathbf{r}}{\partial f \partial g} &= \frac{\mathbf{r} \sin 2L}{\eta_1^2}, \quad \frac{\partial^2 \mathbf{r}}{\partial h \partial k} = \frac{8 h k \mathbf{r}}{\beta^4} + \frac{2 r}{\beta^4} [(2 - \beta^2) \sin L, (2 - \beta^2) \cos L, 2 \eta_6]^T, \\
\frac{\partial^2 \mathbf{r}}{\partial f \partial L} &= \frac{\mathbf{r} \eta_7}{\eta_1} - \frac{\cos L}{\eta_1} \frac{\partial \mathbf{r}}{\partial L}, \quad \frac{\partial^2 \mathbf{r}}{\partial h \partial L} = -\frac{2 h}{\beta^2} \frac{\partial \mathbf{r}}{\partial L} + \frac{2 r}{\beta^2} [\eta_2 \eta_5 - \eta_4, -\eta_2 \eta_4 - \eta_5, \eta_8]^T, \\
\frac{\partial^2 \mathbf{r}}{\partial g \partial L} &= -\frac{\mathbf{r} \eta_8}{\eta_1} - \frac{\sin L}{\eta_1} \frac{\partial \mathbf{r}}{\partial L}, \quad \frac{\partial^2 \mathbf{r}}{\partial k \partial L} = -\frac{2 k}{\beta^2} \frac{\partial \mathbf{r}}{\partial L} + \frac{2 r}{\beta^2} [\eta_2 \eta_4 + \eta_5, \eta_2 \eta_5 - \eta_4, \eta_7]^T
\end{aligned}$$

Since $r = \|\mathbf{r}\| = p / (1 + f \cos L + g \sin L)$, the derivative $dr/d\boldsymbol{\alpha}$ is derived as

$$\frac{\partial r}{\partial \boldsymbol{\alpha}} = \left[\frac{r}{p}, -\frac{r \cos L}{\eta_1}, -\frac{r \sin L}{\eta_1}, 0, 0, r \eta_2 \right]^T$$

References

- [1] F. Zuiani, M. Vasile, A. Palmas, G. Avanzini, Direct transcription of low-thrust trajectories with finite trajectory elements, *Acta Astronautica* 72 (2012) 108–120, doi: 10.1016/j.actaastro.2011.09.011.
- [2] F. Topputo, C. Zhang, Survey of direct transcription for low-thrust space trajectory optimization with applications, *Abstract and Applied Analysis* 2014 (2014) 1–15, doi: 10.1155/2014/851720.
- [3] M. Bassetto, A. A. Quarta, G. Mengali, Trajectory approximation of a passively actuated

- solar balloon in near-earth mission scenarios, *Acta Astronautica* 188 (2021) 451–462, doi: 10.1016/j.actaastro.2021.08.007.
- [4] M. Bassetto, L. Boni, G. Mengali, A. A. Quarta, Electric sail phasing maneuvers with radial thrust, *Acta Astronautica* 179 (2021) 99–104, doi: 10.1016/j.actaastro.2020.10.025.
- [5] J. Kawaguchi, A. Fujiwara, T. Uesugi, Hayabusa—its technology and science accomplishment summary and hayabusa-2, *Acta Astronautica* 62 (10-11) (2008) 639–647, doi: 10.1016/j.actaastro.2008.01.028.
- [6] J. Benkhoff, J. Van Casteren, H. Hayakawa, M. Fujimoto, H. Laakso, M. Novara, P. Ferri, H. R. Middleton, R. Ziethe, Bepicolombo—comprehensive exploration of mercury: Mission overview and science goals, *Planetary and Space Science* 58 (1-2) (2010) 2–20, doi: 10.1016/j.pss.2009.09.020.
- [7] J. T. Betts, Survey of numerical methods for trajectory optimization, *Journal of guidance, control, and dynamics* 21 (2) (1998) 193–207, doi: 10.2514/2.4231.
- [8] L. Cheng, Z. Wang, Y. Song, F. Jiang, Real-time optimal control for irregular asteroid landings using deep neural networks, *Acta Astronautica* 170 (2020) 66–79, doi: 10.1016/j.actaastro.2019.11.039.
- [9] B. A. Conway, A survey of methods available for the numerical optimization of continuous dynamic systems, *Journal of Optimization Theory and Applications* 152 (2) (2012) 271–306, doi: 10.1007/s10957-011-9918-z.
- [10] S. Chen, H. Li, H. Baoyin, Multi-rendezvous low-thrust trajectory optimization using costate transforming and homotopic approach, *Astrophysics and Space Science* 363 (6) (2018) 1–16, doi: 10.1007/s10509-018-3334-x.
- [11] A. E. Petropoulos, J. M. Longuski, Shape-based algorithm for the automated design of low-thrust, gravity assist trajectories, *Journal of Spacecraft and Rockets* 41 (5) (2004) 787–796, doi: 10.2514/1.13095.
- [12] Y. Song, X. Miao, S. Gong, Adaptive powered descent guidance based on multi-phase pseudospectral convex optimization, *Acta Astronautica* 180 (2021) 386–397, doi:

10.1016/j.actaastro.2020.12.019.

- [13] F. Jiang, G. Tang, J. Li, Improving low-thrust trajectory optimization by adjoint estimation with shape-based path, *Journal of Guidance, Control, and Dynamics* 40 (12) (2017) 3282–3289, doi: 10.2514/1.G002803.
- [14] X. Li, D. Qiao, H. Chen, Interplanetary transfer optimization using cost function with variable coefficients, *Astrodynamics* 3 (2) (2019) 173–188, doi: 10.1007/s42064-018-0043-8.
- [15] D. Wu, F. Jiang, J. Li, Warm start for low-thrust trajectory optimization via switched system, *Journal of Guidance, Control, and Dynamics* 44 (9) (2021) 1700–1706, doi: 10.2514/1.G005983.
- [16] F. W. Boltz, Orbital motion under continuous tangential thrust, *Journal of Guidance, Control, and Dynamics* 15 (6) (1992) 1503–1507, doi: 10.2514/3.56583.
- [17] M. Bassetto, A. A. Quarta, G. Mengali, Generalized sail trajectory approximation with applications to magsails, *Aerospace Science and Technology* 118 (2021) 106991, doi: 10.1016/j.ast.2021.106991.
- [18] J. E. Prussing, V. Coverstone-Carroll, Constant radial thrust acceleration redux, *Journal of Guidance, Control, and Dynamics* 21 (3) (1998) 516–518, doi: 10.2514/2.7609.
- [19] M. Bassetto, A. A. Quarta, G. Mengali, V. Cipolla, Spiral trajectories induced by radial thrust with applications to generalized sails, *Astrodynamics* 5 (2) (2021) 121–137, doi: 10.1007/s42064-020-0093-6.
- [20] T. N. Edelbaum, Propulsion requirements for controllable satellites, *Ars Journal* 31 (8) (1961) 1079–1089, doi: 10.2514/8.5723.
- [21] C. Wen, C. Zhang, Y. Cheng, D. Qiao, Low-thrust transfer between circular orbits using natural precession and yaw switch steering, *Journal of Guidance, Control, and Dynamics* (2021) 1–8doi: 10.2514/1.G005790.
- [22] B. J. Wall, B. A. Conway, Shape-based approach to low-thrust rendezvous trajectory design, *Journal of Guidance, Control, and Dynamics* 32 (1) (2009) 95–101, doi: 10.2514/1.36848.

- [23] E. Taheri, O. Abdelkhalik, Initial three-dimensional low-thrust trajectory design, *Advances in Space Research* 57 (3) (2016) 889–903, doi: 10.1016/j.asr.2015.11.034.
- [24] D. M. Novak, M. Vasile, Improved shaping approach to the preliminary design of low-thrust trajectories, *Journal of Guidance, Control, and Dynamics* 34 (1) (2011) 128–147, doi: 10.2514/1.50434.
- [25] A. Caruso, A. A. Quarta, G. Mengali, M. Ceriotti, Shape-based approach for solar sail trajectory optimization, *Aerospace Science and Technology* 107 (2020) 106363, doi: 10.1016/j.ast.2020.106363.
- [26] K. Zeng, Y. Geng, B. Wu, Shape-based analytic safe trajectory design for spacecraft equipped with low-thrust engines, *Aerospace Science and Technology* 62 (2017) 87–97, doi: 10.1016/j.ast.2016.12.006.
- [27] M. Vasile, P. De Pascale, S. Casotto, On the optimality of a shape-based approach based on pseudo-equinoctial elements, *Acta Astronautica* 61 (1) (2007) 286–297, doi: 10.1016/j.actaastro.2007.01.017.
- [28] L. A. Ricciardi, M. Vasile, Direct transcription of optimal control problems with finite elements on bernstein basis, *Journal of Guidance, Control, and Dynamics* 42 (2) (2019) 229–243, doi: 10.2514/1.G003753.
- [29] P. De Pascale, M. Vasile, Preliminary design of low-thrust multiple gravity-assist trajectories, *Journal of Spacecraft and Rockets* 43 (5) (2006) 1065–1076, doi: 10.2514/1.19646.
- [30] D. J. Gondelach, R. Noomen, Hodographic-shaping method for low-thrust interplanetary trajectory design, *Journal of Spacecraft and Rockets* 52 (3) (2015) 728–738, doi: 10.2514/1.A32991.
- [31] D. Wu, L. Cheng, F. Jiang, J. Li, Rapid generation of low-thrust many-revolution earth-center trajectories based on analytical state-based control, *Acta Astronautica* 187 (2021) 338–347, doi: 10.1016/j.actaastro.2021.05.017.

- [32] J. T. Betts, Very low-thrust trajectory optimization using a direct sqp method, *Journal of Computational and Applied Mathematics* 120 (1-2) (2000) 27–40, doi: 10.1016/S0377-0427(00)00301-0.
- [33] G. H. Behforooz, N. Papamichael, End conditions for cubic spline interpolation, *IMA Journal of Applied Mathematics* 23 (3) (1979) 355–366, doi: 10.1016/0096-3003(90)90125-M.
- [34] M. J. Powell, A direct search optimization method that models the objective and constraint functions by linear interpolation, in: *Advances in Optimization and Numerical Analysis*, Springer, Dordrecht, 1994, pp. 51–67.
- [35] H. Yang, S. Li, X. Bai, Fast homotopy method for asteroid landing trajectory optimization using approximate initial costates, *Journal of Guidance, Control, and Dynamics* 42 (3) (2018) 585–597, doi: 10.2514/1.G003414.
- [36] X. Zeng, X. Liu, Searching for time optimal periodic orbits near irregularly shaped asteroids by using an indirect method, *IEEE Transactions on Aerospace and Electronic Systems* 53 (3) (2017) 1221–1229, doi: 10.1109/TAES.2017.2668071.
- [37] W. Wang, D. Wu, G. Mengali, A. A. Quarta, H. Baoyin, Asteroid hovering missions from a fuel-consumption viewpoint, *Journal of Guidance, Control, and Dynamics* 43 (7) (2020) 1374–1382, doi: 10.2514/1.G005016.
- [38] E. Taheri, J. L. Junkins, Generic smoothing for optimal bang-off-bang spacecraft maneuvers, *Journal of Guidance, Control, and Dynamics* 41 (11) (2018) 2470–2475, doi: 10.2514/1.G003604.
- [39] D. Wu, Y. Song, Z. Chi, E. Zhibo, H. Sun, H. Baoyin, F. Jiang, Problem a of the 9th china trajectory optimization competition: Results found at tsinghua university, *Acta Astronautica* 150 (2018) 204–212, doi: 10.1016/j.actaastro.2018.06.001.
- [40] F. Jiang, H. Baoyin, J. Li, Practical techniques for low-thrust trajectory optimization with homotopic approach, *Journal of Guidance, Control, and Dynamics* 35 (1) (2012) 245–257, doi: 10.2514/1.52476.